Spatial Characteristics of Visual Field Progression Determined by Monte Carlo Simulation: Diagnostic Innovations in Glaucoma Study

John P. Pascual,[1] *Ulrich Schiefer,*[2] *Jens Paetzold,*[2] *Linda M. Zangwill,*[1] *Ivan M. Tavares,*[3] *Robert N. Weinreb,*[1] *and Pamela A. Sample*[1]

Purpose. To determine the spatial characteristics of glaucomatous visual field progression in persons with glaucomatous-appearing optic neuropathy (GON) from the Diagnostic Innovations in Glaucoma Study (DIGS).

Methods. Changes in pattern deviation (PD) plot values from the average of two baseline examinations to two follow-up examinations were evaluated in test locations. All were eligible, full threshold, pattern 24-2, standard automated perimetry (SAP) examinations (Humphrey Field Analyzer II; Carl Zeiss Meditec, Inc., Dublin, CA) in visual field series from 200 patients with GON confirmed on two occasions by stereophoto review. The proportion of patients exhibiting PD plot progression was determined at each of 52 locations for patients with a baseline abnormal result ($P < 5\%$ or worse) in one or more of 52 PD locations in either the first or second baseline test for a total of 2704 location pairings for each possible level of negative PD change from −1 to −50 dB. Progression was defined as any worsening of PD plot value in the follow-up test relative to the average PD plot value in the baseline tests. Monte Carlo simulation was used to determine the significance of the observed patterns of PD plot progression.

Results. Changes in PDs were dependent on their location relative to abnormal PD locations in the first test. Of those patients with an abnormality at a location at baseline (mean, 0.23 ± 0.07), the proportion of patients changing by –2 dB or more ranged between 0.09 and 0.55 (mean, 0.29 ± 0.06) across locations. For changes of −6 dB or more, the proportions ranged between 0.00 and 0.26 (mean, 0.08 ± 0.04) of patients. These proportions and the proportional probabilities for each of 2704 location pairings are reported for selected levels of change. The proportional probabilities are consistent with a map of the retinal nerve fiber layer bundles.

Conclusions. Visual field progression occurs in retinotopically constrained patterns consistent with changes along the nerve fiber bundle. (*Invest Ophthalmol Vis Sci.* 2007;48:1642–1650) DOI:10.1167/iovs.06-0966

Clinical intervention in glaucoma is concerned with halting or slowing progression of the disease. Integral to this goal is the tracking of disease progression. Clinically, visual field testing can be used to provide an assessment of functional changes. These functional changes are related to the underlying health of the retinal ganglion cells. Weber and Ulrich[1] quantified this relationship, building a map of locations whose defects were related to specific scotoma patterns, approximating the nerve fiber bundle projections. More recently, Garway-Heath et al.[2] have also developed a mapping of the relationship between the nerve fiber layer bundles and the visual field in patients with normal-tension glaucoma. The goal of the present study is to assess whether longitudinal changes also obey these projections such that change is more likely to occur in regions along the same nerve fiber bundles where damaged locations exist.

Determining the spatial patterns of visual field progression may help improve progression algorithms. Most visual field progression algorithms do not take into account the spatial pattern of changes. Statpac's Glaucoma Change Probability[3,4] and the Glaucoma Progression Analysis (GPA), the latter born from the Early Manifest Glaucoma Trial (EMGT) progression algorithm,[5] rely on repeatability of multiple negative point-wise changes to thresholds on either the total deviation (TD) or pattern deviation (PD) plot, but do not require any additional spatial criteria for calling progression. Point-wise linear regression analysis (PLRA) techniques, such as that implemented by the Progressor software (Moorfields Eye Hospital, London, UK, Medisoft Ltd., Leeds, UK),[6] are also concerned with point-wise changes of the threshold plot, and similarly do not impose any spatial criteria for progression. The Collaborative Initial Glaucoma Treatment Study (CIGTS) uses a score obtained by summing the convolution of a scoring algorithm over a numerically transformed TD probability plot.[7] By virtue of the scoring procedure, the CIGTS score does not fully account for the relationship of distant defective locations and merely discounts singular defects that are not adjacent to TD defects. The algorithm that comes closest to accounting for spatial relationships is the Advanced Glaucoma Intervention Study (AGIS). It applies a complex scoring algorithm to defect patterns in separate regions of the visual field.[8] Though AGIS takes into account spatial relationships, the regions are few in number, rather broad, and nonspecific for any particular spatial pattern of progression. In addition, the obtained score is heuristic since the scoring method was developed subjectively. For a review of these progression algorithms, see Spry and Johnson.[9]

Determining the spatial characteristics of visual field progression may help development of more sensitive progression algorithms. In a previous study of cross-sectional data, Monte Carlo simulation was used to illustrate common defect-patterns across a glaucomatous population (Hu A, et al. *IOVS* 2005;46: ARVO E-Abstract 3734). In this study, Monte Carlo simulation is

From the [1]Hamilton Glaucoma Center, University of California at San Diego, La Jolla, California; the [2]University Eye Hospital, Department II, Tübingen, Germany; and the [3]Federal University, São Paulo, Brazil.

Supported by National Eye Institute Grants EY08208 (PAS) and EY 11008 (LMZ). Participant retention incentive grants in the form of glaucoma medication at no cost were provided by Alcon Laboratories, Inc., Allergan, Pfizer, Inc., and Santen, Inc.

Submitted for publication August 14, 2006; revised December 8, 2006; accepted February 16, 2007.

Disclosure: **J.P. Pascual**, None; **U. Schiefer**, Haag-Streit (F,P,R); **J. Paetzold**, Haag-Streit (F); **L.M. Zangwill**, Carl-Zeiss Meditec (F,R); **I.M. Tavares**, None; **R.N. Weinreb**, Carl-Zeiss Meditec (F,R); **P.A. Sample**, Carl-Zeiss Meditec (F), Haag-Streit (F), Welch Allyn (F)

The publication costs of this article were defrayed in part by page charge payment. This article must therefore be marked "*advertisement*" in accordance with 18 U.S.C. §1734 solely to indicate this fact.

Corresponding author: Pamela A. Sample, Department of Ophthalmology, University of California, San Diego, 9500 Gilman Drive, La Jolla, CA 92093-0946; psample@glaucoma.ucsd.edu.

used to quantify the spatial relationship of visual field changes in longitudinal series from patients with glaucoma, and these patterns are compared to Weber's nerve fiber bundle map. Progression is evaluated between locations that exhibit defects on initial tests and the thresholds in follow-up tests across time for all test locations.

METHODS

Participants

Participants were from a longitudinal study of visual function in glaucoma, The Diagnostic Innovations in Glaucoma Study (DIGS), at the Hamilton Glaucoma Center, University of California, San Diego. This study conforms to the tenets of the Declaration of Helsinki and the Health Insurance Portability and Accountability Act of 1996 (HIPAA) and was approved by the Human Subjects Committee at the University of California, San Diego. The nature of the procedures was explained, and informed consent was obtained from all participants.

Inclusion Criteria for DIGS. All participants underwent complete ophthalmic examination including slit lamp biomicroscopy, intraocular pressure measurement, dilated stereoscopic fundus examination, and stereophotography of the optic nerve heads. Simultaneous stereoscopic photographs were obtained in all participants and were of adequate quality for the participant to be included. At study entry, all participants had open angles, a best corrected acuity of 20/40 or better, a spherical refraction within ±5.0 D, and cylinder correction within ±3.0 D. A family history of glaucoma was allowed.

Exclusion Criteria for DIGS. Participants were excluded if they had a history of intraocular surgery (except uncomplicated cataract surgery). Also excluded were all participants with elevated intraocular pressure secondary to causes other than glaucoma (e.g., iridocyclitis, trauma), other intraocular eye disease, other diseases affecting the visual field (e.g., pituitary lesions, demyelinating diseases, HIV or AIDS, or diabetic retinopathy), medications known to affect visual field sensitivity or problems other than glaucoma affecting color vision.

Inclusion Criteria for this Study. DIGS includes healthy eyes and eyes with ocular hypertension, suspected glaucoma, and diagnosed glaucoma. For this study, only the DIGS participants with at least four reliable full-threshold, pattern 24-2, standard automated perimetry (SAP) tests performed on the Humphrey Field Analyzer (Carl-Zeiss Meditec, Dublin, CA) and at least two stereophotographs indicative of glaucomatous optic neuropathy (GON) any time during follow-up were considered for inclusion in this study.

Four, reliable SAP full-threshold examinations were chosen for inclusion, with two serving as baseline examinations and the other two serving as follow-up examinations. If more than four examinations in a visual field series from a patient were eligible for inclusion, the earliest two tests performed within the shortest amount of time of each other were chosen for inclusion as baseline examinations and the latest two examinations were chosen as follow-up examinations. If only four examinations were eligible, the first two examinations were chosen as the baseline examinations, and the last two were chosen as the follow-up examinations. SAP reliability was defined as fewer than 33% fixation loss or false-positive or -negative errors. Because PD plots would be used for subsequent analyses, persons with baseline visual fields that had severe or end-stage loss as defined by the Hodapp-Anderson-Parrish criteria[10] were excluded because the PD plot can appear normal at the more advanced stages of the disease.[11]

GON diagnoses were based on masked, independent review of simultaneous color stereophotographs of the optic nerve head by two trained graders from the Optic Disc Reading Center, UCSD. When graders disagreed, a third expert adjudicated. GON was defined as the presence of excavation, neuroretinal rim thinning or notching, nerve fiber layer defects, or an asymmetry of the vertical cup-to-disc ratio ≥0.2 between the two eyes. Stereophotographs were obtained (TRC-SS camera; Topcon Instrument Corp. of America, Paramus, NH) after maximum pupil dilation and were assessed with a stereoscopic viewer (Pentax Stereo Viewer II; Asahi Optical Co., Tokyo, Japan). Intraocular pressure was not used for inclusion or exclusion of subjects.

Exclusion Criteria for this Study. Any DIGS participants with intraocular eye surgery, including glaucoma surgery, during the time between their first and last eligible visual field tests were excluded.

Standard Automated Perimetry

SAP full threshold obtains luminance threshold estimates according to a 4-2-2 staircase algorithm with two reversals applied to 54 locations spaced 6° apart in the pattern 24-2 test grid. The locations in the visual field are tested in a pseudorandom fashion by using stimuli that subtend 0.43° of visual angle, modulated between 0.1 and 10,000 asb (0.032 and 3183 cd/m^2) on a 31.6-asb (10.06 cd/m^2) background, allowing for a testing range of 50 dB.[3]

The PD plot is derived from the obtained luminance thresholds and accounts for changes in media opacity and other factors, such as miotic pupils, that affect the thresholds at all test locations. To accomplish this, the deviations of thresholds from the mean of age-corrected thresholds in normal subjects, the TDs, are ranked from least to most sensitive. The general sensitivity, which is the seventh most sensitive TD, is subtracted from all the age-corrected thresholds in the visual field to obtain the numerical PD plot. A grayscale plot of PD probabilities is generated by comparing the PDs to one tail of the distribution of PDs from the perimeter's internal, normative database. Lower PD probabilities (e.g., $P < 5\%$, $P < 1\%$, and $P < 0.5\%$) are indicative of a deviation from normal function, possibly due to glaucomatous damage.[12]

Determining Patterns of Change

The procedure for determining PD plot changes is illustrated in Figure 1. The two locations approximating the location of the blindspot were excluded from subsequent analyses. For all the patients with a defect in location 1 (PD $P < 5\%$) on either of the baseline visual field tests, each location (locations 1–52) was evaluated for a change in PD between each of the two follow-up examinations from the location's average PD in the two baseline examinations, with each follow-up examination treated independently. The number of PD changes recorded at each location in each of the follow-up examinations, therefore, equaled twice the number of patients abnormal at location 1 on at least one of their baseline examinations (two follow-up examinations per patient). Next, all patients with a defect in location 2 on either baseline test were evaluated for PD changes in every location in both of their follow-up visual field tests. These comparisons were repeated for all 52 locations in each patient for any defective locations in the baseline tests, for a total of 2704 (52 × 52 locations) possible comparisons. For each of the 52 locations, the proportions of fields with PDs that worsened for a given defective location in the baseline tests were determined for each possible level of negative change (i.e., −1, −2, −3,. . . −50 dB).

Monte Carlo Simulation

In this study, the spatial relationships between PD changes and existing abnormalities were of interest. Two competing hypotheses may account for the results (1) the observed PD changes have no spatial relationship to existing defects and are only the result of an overall worsening of the visual field, or (2) the observed changes obey spatial patterns. To evaluate these hypotheses, Monte Carlo simulations were performed to obtain the probabilities that the observed progression was significant. Monte Carlo simulations are a useful, nonparametric method for obtaining inferential statistics for variables with unknown sampling distributions.[13] In this study, the Monte Carlo simulations were used to compare the observed proportions of changes in PDs to a simulated population of fields with PD changes that obey no underlying spatial relationship (i.e., random changes throughout the whole visual field).

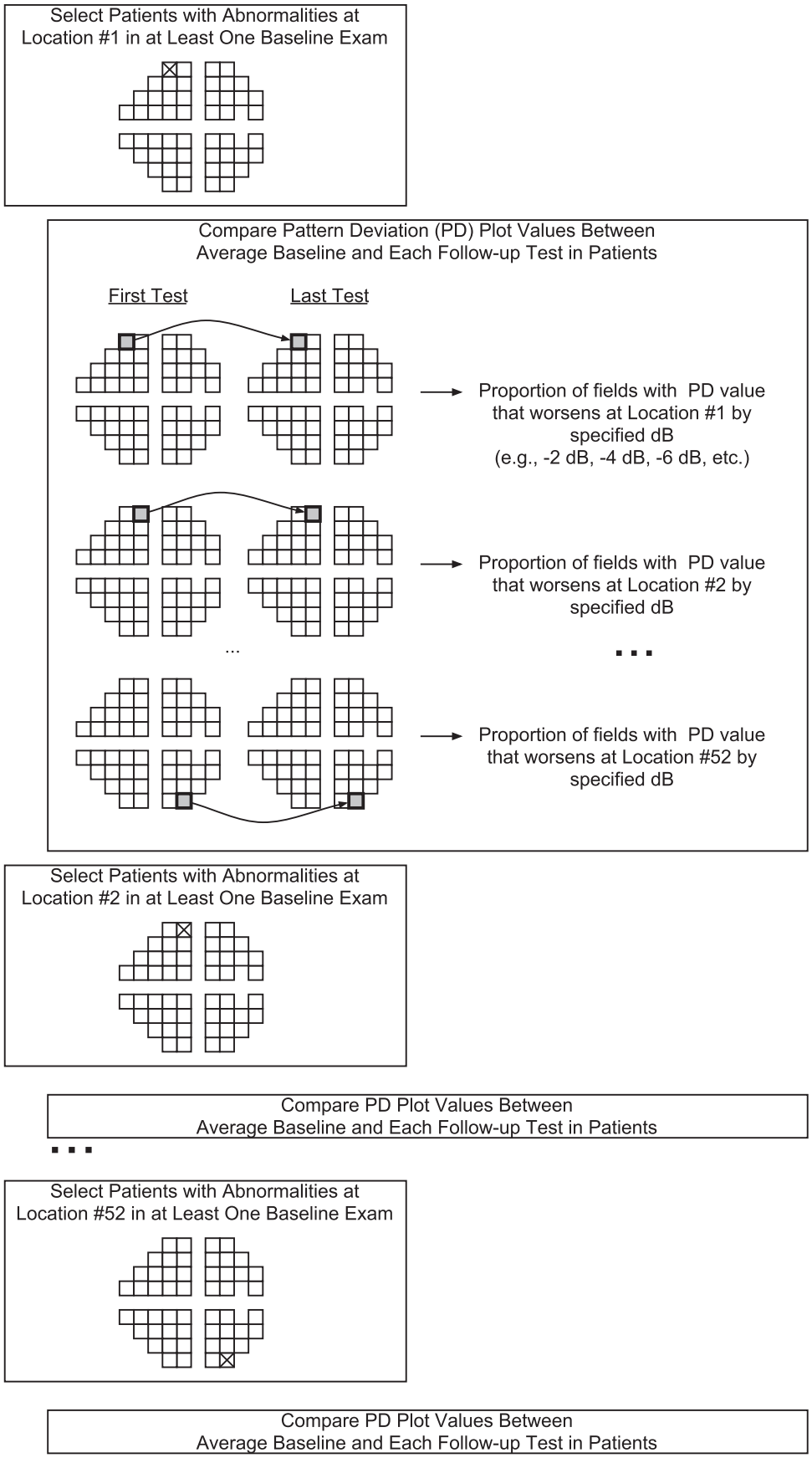

FIGURE 1. Method for determining the proportion of patients whose PDs worsen at each location in the pattern 24-2 test grid for a given defective location in the first test.

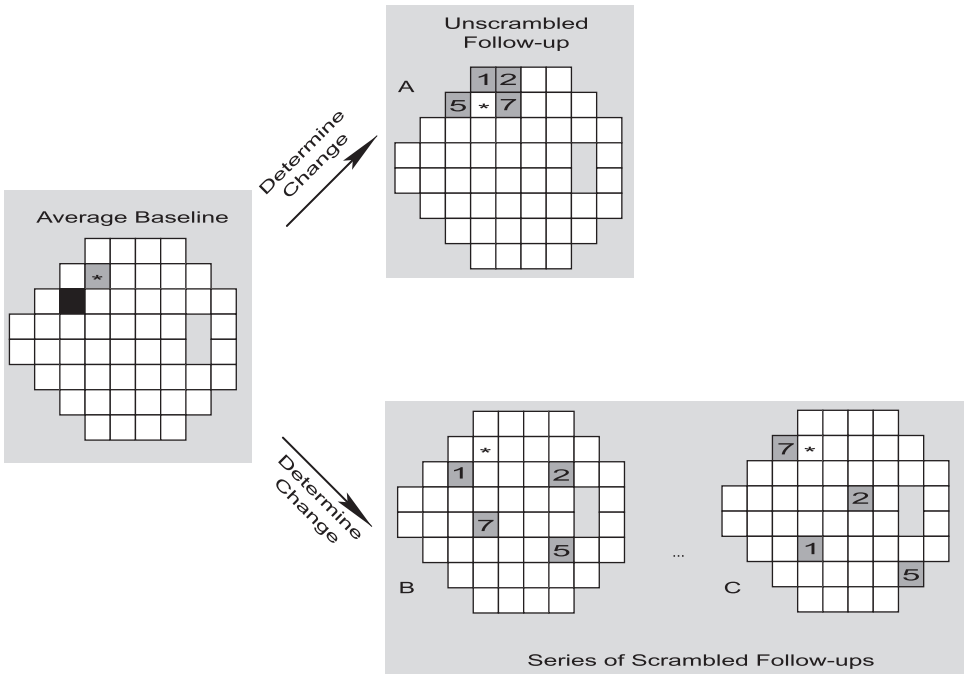

FIGURE 2. The PDs of the locations in the average baseline field were compared to those in the locations in each follow-up field. (**A**) Progression occurred in the unscrambled follow-up field in locations 1, 2, 5, and 7 when the *asterisked* location was abnormal at baseline. (**B**) The locations were scrambled, and the locations are re-evaluated for change. Notice that location 1 was no longer considered to be progressing because it was no longer worse than the PD at that location in the average baseline examination. (**C**) The follow-up field was scrambled 100,000 times in total.

Monte Carlo simulations maintain the same magnitude of changes, but obliterate any potential spatial relationship between these changes. The PDs in follow-up examinations are scrambled so that any location in the visual field is free to replace any other location (Fig. 2). By scrambling the locations in 100,000 iterations, the Monte Carlo simulation obtained frequency distributions of PD changes for each location in the pattern 24-2 test grid, given a defective location in the baseline tests when the locations in the follow-up tests were repeatedly scrambled. The scrambled fields are related to the two competing hypotheses: If the first hypothesis is correct and there is no spatial relationship between changes in the visual field, then the observed proportions should be similar to the proportions of patients that change by the specified amount when the PD was scrambled in follow-up examinations. When compared with the distribution of PD changes, the proportion in the unscrambled case should be close to the mean of proportions in the scrambled cases. However, if the second hypothesis is correct and there is a spatial relationship of change, then the observed proportions in unscrambled fields should be markedly different from those obtained in scrambled follow-up examinations, and the proportion from the unscrambled case should be further along the tail of the distribution of proportions from the scrambled cases, as these are values not likely to be obtained in fields where change is spatially random.

Probabilities can be obtained showing that the true, unscrambled PD changes could be obtained if the patterns of progression are not spatially constrained and occur at random across the visual field. These probabilities are equivalent to the percentile ranks of the PD changes in the unscrambled fields along the distribution of changes at a given decibel level in 100,000 scrambled fields for each patient. An example of a distribution of changes for changes worse than −2 dB at one location for a given abnormal location at baseline is shown in Figure 3. The probabilities for chance occurrence will be small (closer to 0) for those locations whose changes are spatially related to existing abnormalities. These values, while technically probabilities, shall be referred to as "proportional probabilities" to avoid confusion with the PD probabilities.

For post hoc analysis, both the proportions of fields exhibiting change and the proportional probabilities for those proportions were compared to the retinal nerve fiber layer bundle map developed by Weber et al.[1,14] (Fig. 4) to determine whether the patterns of progression identified were consistent with those that would be expected if change is occurring within a given nerve fiber bundle. The proportion of fields progressing within a bundle was compared to the proportion progressing outside the bundle using Wilcoxon's rank sum test, a nonparametric analog to the Student's *t*-test.

RESULTS

From DIGS, 200 eyes from 200 patients met the inclusion criteria for this report. Changes in PDs at each location in the visual field between the average baseline examination and follow-up examination were dependent on the location's po-

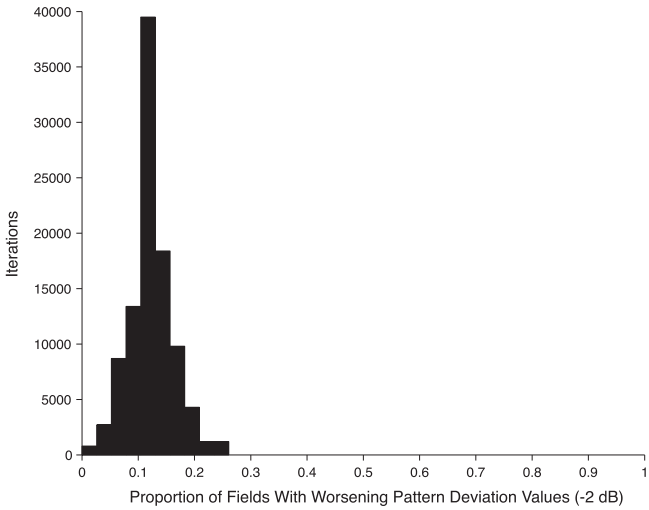

FIGURE 3. An example of a probability mass function (pmf) for the proportion of patients whose PDs worsened across 100,000 iterations of the Monte Carlo simulation. The observed proportion was compared to the pmf to determine the probability that observed proportion could have been obtained from a visual field with changes that had no spatial relationship to already abnormal locations. This example is from patients with PDs that were worsening by −2 dB or more at a location 3° superior, 9° nasal when they had an abnormal PD probability at a location 21° superior, 9° temporal.

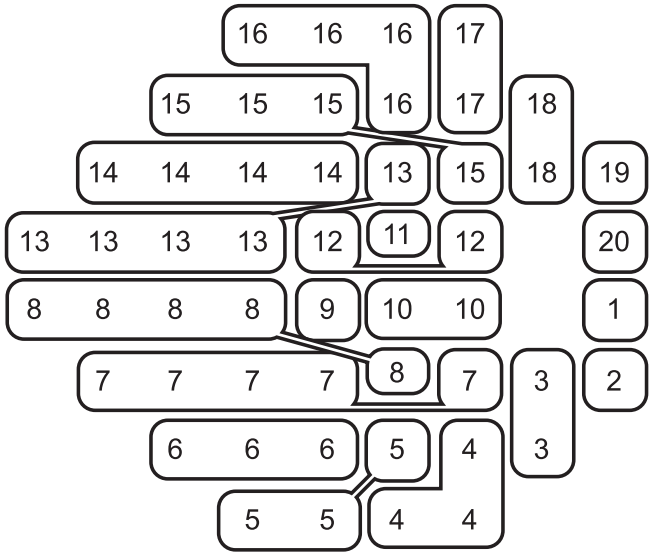

FIGURE 4. Nerve fiber bundles determined by Weber et al.[1,14]

sition relative to abnormal PD locations in the baseline tests. Figures 5 and 6 illustrate two levels of PD change (−2 and −6 dB), along with the proportional probabilities for two different locations that were defective at baseline. Figure 5A illustrates the proportion of fields whose PD worsened by −2 dB or more when the asterisked location was defective in one of the baseline examinations. The darker regions are areas that had more progressing patients and the lighter areas had fewer progressing patients. Figure 5B is similar to Figure 5A, except that it shows the proportion of patients that changed by −6 dB or more. Figure 5C illustrates the proportional probabilities: the probability that the proportions shown in Figure 5A could be generated in a visual field series with locations spatially scrambled in follow-up tests. The darker areas are associated with lower probabilities, and by inference, are less likely to be obtained in fields whose changes occur randomly. These regions are indicative of changes that have a spatial relationship to the asterisked location. The probabilities are lowest in the upper hemifield and nasal-step regions nearest the asterisked location. The region bounded by the outline represents the nerve fiber layer bundle from Weber et al.[1,14] The bounded area tends to have lower probability than other locations, but also appears to be associated with the nasal step. Figure 5D is similar to Figure 5C except that it shows the proportional probabilities for changes of −6 dB or more (Fig. 5B). Figure 6 shows another relationship between visual field locations and a defective location (asterisk) at baseline for two levels of PD change (−2 and −6 dB). The area of change observed in this study matches well with the area predicted by the nerve fiber layer bundle map. Of those patients with an abnormality at a location at baseline (mean, 0.23 ± 0.07), the proportion of patients changing by −2 dB or more ranged between 0.09 and 0.55 (mean, 0.29 ± 0.06) across locations. For changes of −6 dB or more, the proportions ranged between 0.00 and 0.26 (mean, 0.08 ± 0.04) of patients.

The median time between baseline examinations was 0.6 years (25th percentile, 0.4 years; 75th percentile, 1.0 year; range, 0.0–2.5 years), and the median time between the last baseline and the last follow-up tests was 3.0 years (25th percentile, 2.1 years; 75th percentile, 5.0 years; range. 0.4–13.7). The median age at the first test was 65 years (25th percentile, 55 years; 75th percentile, 73 years; range, 24–88). Medians for these variables are reported because of the skew of each of the distributions. The characteristics of the first baseline visual fields are summarized in Table 1. There were more patients abnormal in the superior locations than in the inferior locations in the baseline examinations (Student's *t*-test, $P < 0.001$), but within patients, the median number of abnormal locations at baseline was similar for both hemifields (Wilcoxon signed rank test, $P = 0.06$).

Figure 7 summarizes the proportions of fields changing for two levels of PD changes (−2 and –6 dB) and Figure 8 illustrates the associated proportional probabilities at each of the

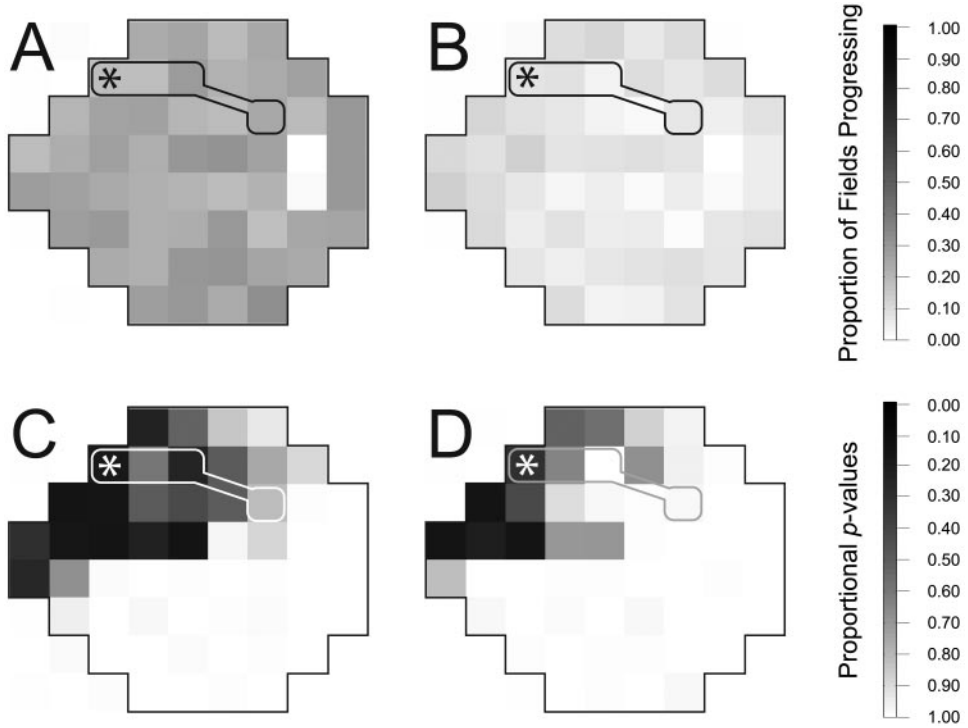

FIGURE 5. (**A**) An example of a superior defect in the baseline test (✶) of 54 patients and the proportion of fields ($n = 108$) with PDs that worsened at each of the 52 locations by −2 dB or more. The darker the location, the more patients exhibited progression in that region when the *asterisked* location was defective in the baseline test. The region bounded by an outline represents the corresponding retinal nerve fiber layer bundle. (**B**) Similar to (**A**), except that the change was −6 dB or more. (**C**) Location-specific probability that the proportions (proportional probabilities) shown in (**A**) could be generated in a visual field series of follow-up tests in which the locations were spatially scrambled. Lower probabilities are indicated by darker locations. The progression in these locations is more likely to be spatially related to the *asterisked* defect in the initial test. In this case, the worsening occurred in other superior locations. (**D**) Similar to (**C**), except the proportional probabilities are illustrated for changes in Figure (**B**) of −6 dB or more.

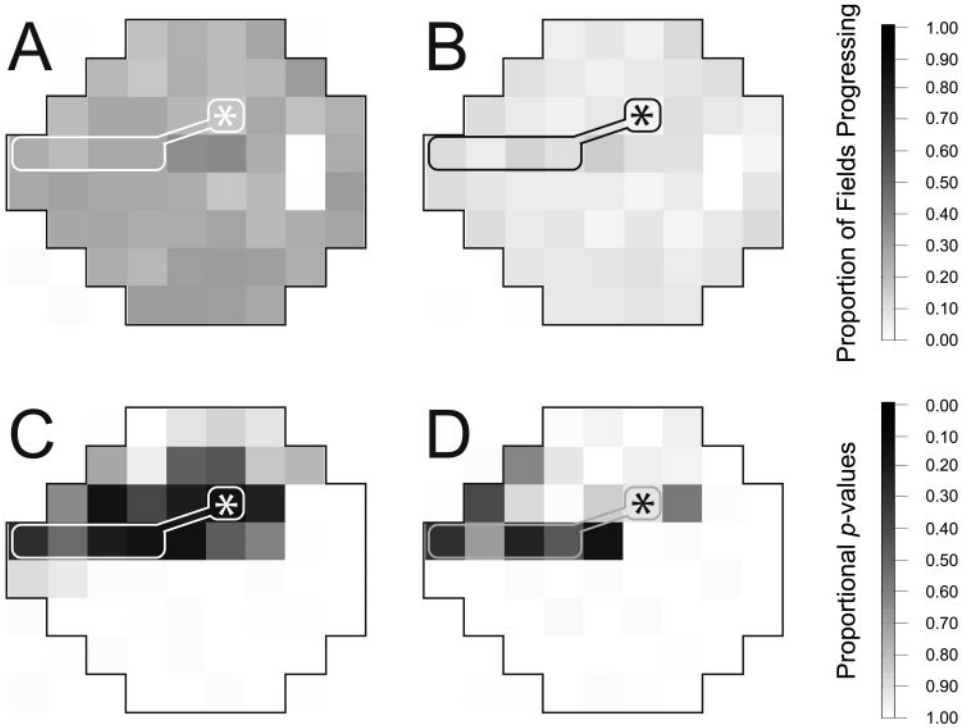

FIGURE 6. (**A**) An example of a superior defect in the baseline test (✶) of 62 patients and the proportion of fields ($n = 124$) whose PDs worsened at each of the 52 locations by −2 dB or more. The darker the location, the more patients exhibit progression in that region when the *asterisked* location is defective in the baseline test. The region bounded by an outline represents the corresponding retinal nerve fiber layer bundle. (**B**) Similar to (**A**), except that the change is −6 dB or more. (**C**) location-specific probability that the proportions (proportional probabilities) shown in (**A**) could be generated in a visual field series whose follow-up tests had their locations spatially scrambled. Lower probabilities are indicated by darker locations. The progression in these locations was more likely to be spatially related to the *asterisked* defect in the initial test. In this case, the worsening occurred in other superior locations. (**D**) Similar to (**C**), except the proportional probabilities are illustrated for changes in Figure 6B of −6 dB or more.

52 locations for a defect in a given location at baseline. In general, the proportions of fields changing do not appear to obey any strong spatial pattern (Fig. 7). However, the proportional probabilities do demonstrate specific patterns (Fig. 8). The difference in patterns between the proportions of fields changing and their proportional probabilities is illustrated in Figures 5 and 6.

Some locations were associated with changes along nerve fiber bundle patterns, as shown by Figure 8. The proportional probabilities for the neighboring locations follow a similar pattern. These patterns were more common in superior locations and less common in inferior locations.

In the post hoc analysis, in general, the patterns followed the retinal nerve fiber layer bundle patterns developed by Weber et al.[1,14] The proportions of patients exhibiting change of –2 dB or more in locations along the same nerve fiber layer bundle were similar to those on different bundles, with medians of 0.29 for both groups of locations (Wilcoxon rank sum, $P = 0.13$). However, the proportional probabilities were lower for locations along the same nerve fiber layer bundle (median = 0.17) than along different nerve fiber bundles (median = 0.66; Wilcoxon rank sum, $P < 0.0001$) indicating the associations were not likely by chance. Changes of –2 dB or more were chosen for post hoc analysis because they exhibited the least clear spatial patterns by either proportions of patients changing or proportional probabilities.

Progression in the nasal step region was common for most of the superior defects and some inferior defects. Figure 8 illustrates the patterns of PD changes for −2 dB or more (Fig. 8A) and −6 dB or more (Fig. 8B) when a nasal region defect was present in the initial test. Superior nasal defects were associated with lower proportional probabilities in the superior hemifield and some inferior nasal locations. The inferior nasal defects, however, were associated with both the superior and inferior nasal area defects.

DISCUSSION

The purpose of this study was to quantify the likelihood of future progression in all visual field locations relative to an initial baseline defect in patients with confirmed GON. There is no gold standard for glaucoma progression. Current progression algorithms were developed using test–retest confidence intervals from baseline tests in clinical trials[7,8] or patients with "stable" glaucoma[4] who were tested within a short period when glaucoma is not likely to progress. Therefore, the definitions of progression for these algorithms are based on con-

TABLE 1. Characteristics of the Baseline Visual Field Examinations

	Mean Deviation (First Baseline)*	Pattern Standard Deviation (First Baseline)*	Proportion of Patients with PD $P < 5\%$ across Locations (Mean ± SD)	Average Number of Locations with PD $P < 5\%$ across Patients*
Overall	−1.87 (−5.08, −0.60)	2.47 (1.93, 5.99)	0.23 ± 0.07†	9 (4–19)†
Superior	—	—	0.26 ± 0.06‡	4 (1–10)‡
Inferior	—	—	0.20 ± 0.06‡	4 (1–8)‡

* Since the distributions are skewed, values given as median (25th percentile, 75th percentile).
† Across 52 locations.
‡ Across 26 locations.

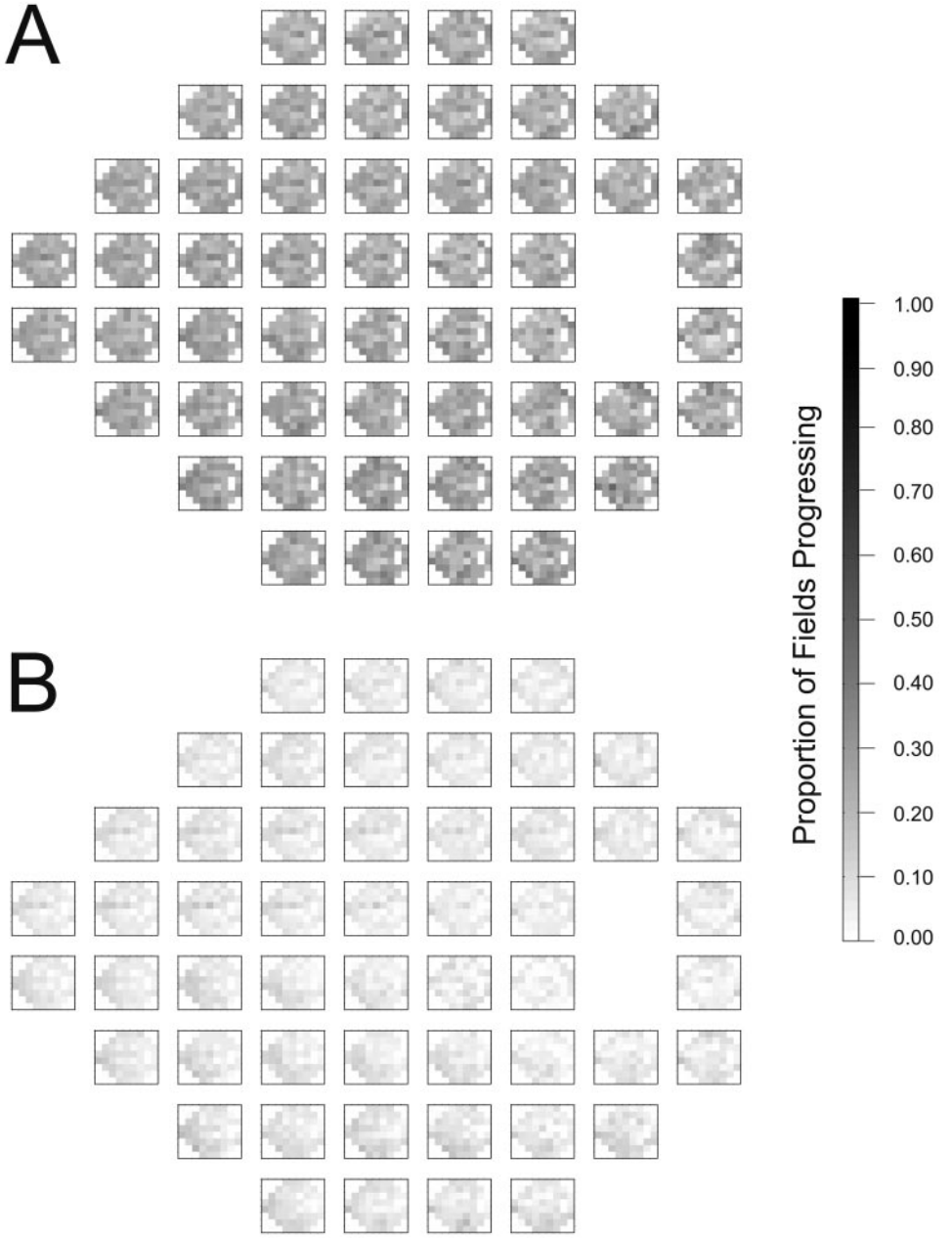

FIGURE 7. Proportion of patients progressing at each of 52 locations when a location was defective in the first test. Each box represents one of the 52 visual field locations. The defective location in the first test is given by the position of the box. Within each box is a visual field that represents the proportions of patients whose PD probabilities progressed at each of the 52 locations. The darker regions are locations where more patients progressed. (**A**) Proportions for changes of −2 dB or more. (**B**) Proportions for changes of −6 dB or more. The visual fields within each box can be thought of as "thumbnail" versions of Figures 5A, 5B, 6A, and 6B. Figure 5A would be the first box from the left on the second row from the top in Figure (**A**). Figure 5B would be the first box from the left on the second row from the top in Figure 7B. Figure 6A would be the fifth box from the left on the third row from the top in (**A**), and Figure 6B would be the same box in (**B**).

fidence intervals for stability and not physiological progression. These algorithms do not capitalize on the spatial patterns of change, which could enhance their sensitivity for change. Gardiner et al.[15] have demonstrated that applying physiologically derived spatial filters to individual visual fields within a series can increase sensitivity to progressive changes. Although, in both research and clinical practice, looking for adjacent locations to worsen to be certain of progression has been evaluated, the method presented herein provides a valid approach for assessing the importance of both proximal and distal points along a nerve fiber bundle for their relevance in observing glaucomatous change in visual fields. In addition, future scoring methods can use these spatial relationships to predict the most likely relationship of future defects relative to the defects found in baseline visual fields. Furthermore, these patterns may serve as a guide for adding test points to individualize follow-up testing by using a condensed perimetric grid within the regions most likely to progress (Paetzold J, et al. *IOVS* 2005;46:ARVO E-Abstract 636).

The results of this study show a spatial relationship between initially defective locations found at baseline and those found on subsequent testing and were similar to those observed in a Monte Carlo simulation that was used to analyze fields from a cross-sectional group of patients with visual function defects (Hu A, et al. *IOVS* 2005;46:ARVO E-Abstract 3734). In addition to being consistent with clinical impressions, the Monte Carlo methods used were able to quantify these spatial relationships. In this study population, superior defects are related to progression in superior locations, with defects related to nerve fiber bundle patterns. The inferior defects also demonstrated specific patterns of progression, but not as clearly as the superior defects. The nasal step region is an important region, as it progressed relative to a number of locations that exhibited a defect in initial visual field tests. These results may not hold for a sample with more advanced glaucomatous defects where change in these locations may already be at the end of the testable range of the perimeter.

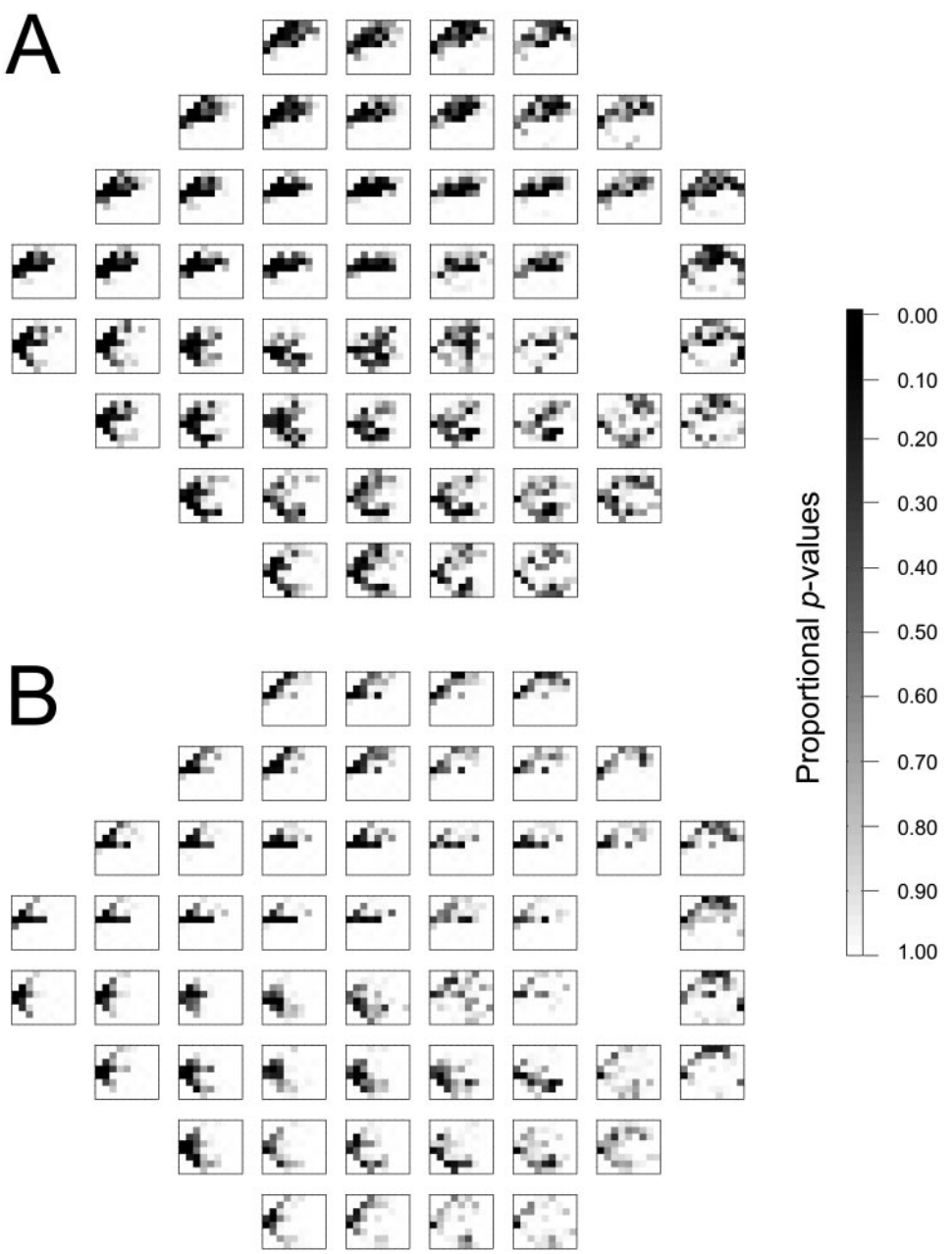

FIGURE 8. Proportional probabilities for the plots in Figure 7. Similar to Figure 7, each box represents one of the 52 visual field locations. The defective location in the first test is given by the position of the box. Within each box is a visual field that represents the probability that the progression in Figure 7 could be generated in a visual field series whose follow-up tests had their locations spatially scrambled. Lower probabilities are indicated by darker locations. The progression in these locations is more likely to be spatially related to the *asterisked* defect in the initial test. (**A**) Proportional probabilities for changes of −2 dB or more. (**B**) Proportional probabilities for changes of −6 dB or more.

The proportion of patients with progressive disease did not appear to differ across locations as distinctly as the proportional probabilities. This may be due to the variability of measurements affecting the proportions. Variability may cause locations to appear to change across patients, masking the true proportions of change. The Monte Carlo analysis solves this dilemma: When locations are scrambled, unrelated normal locations may be replaced by worse PDs, resulting in progression in the scrambled-field series. Comparing the actual unscrambled fields to this distribution reveals the likelihood that the observed proportion of progression could be obtained by chance. This method is especially useful in peripheral locations where the variability is greater than in locations closer to fixation. Assessment of these probabilities facilitates the ability to see true relationships between the test locations, as shown in Figure 8. Thus, while the proportions of progression may appear homogenous across the field, it is the pattern of the proportional probabilities that allows separation of progression from variability.

The use of Monte Carlo simulation is perhaps the least biased method for determining the relationships between locations with changing PDs. Since each location that was defective was compared to changes in every other location in the visual field, neither neighboring locations nor distal locations were considered differently, but rather they were given an equal a priori likelihood of having a spatial relationship to the defective location in the initial test. The observed spatial relationships "fall out" of the data and are not due to manipulations or assumptions placed on the data. It is noteworthy, therefore, that the observed patterns are similar to the retinal nerve fiber layer patterns calculated from numerous visual fields by Weber et al.,[1,14] since they selected for physiological defects and applied spatial constraints to the functional data when deriving their map, whereas this study did not use any such specific defects or spatial constraints to construct the observed patterns. The patterns of progression found in this study could be improved by stratifying the results by the amount or magnitude of defect in baseline examinations, but this would require a

larger number of patients who exhibit the requisite defect depth or defect patterns at baseline.

The results of the Monte Carlo simulation may also, in part, reflect a perimetry-specific component of change in addition to the actual changes due to glaucoma. The SAP full-threshold 24-2 algorithm uses a growth pattern in which the thresholds of seed locations influence the start value of the staircase thresholding procedure in adjacent locations, which in turn can influence the obtained thresholds. Although it is not possible to tease out this perimetry-specific component from the results, it is worth noting the possibility of its existence as it may have utility in the development or improvement of perimetric techniques for tracking progression.

Earlier work defined progression using longitudinal assessment of stereophotographs (Pascual JP, et al. *IOVS* 2005;46: ARVO E-Abstract 3712)[16]; however, the number of patients in our study exhibiting such progression was not enough to allow Monte Carlo analysis. For this reason, the earliest and latest visual field test results in patients with confirmed GON were used. It was hypothesized that the tests bracketed a time frame where true progression occurred in some proportion of patients.

The spatial resolution afforded by the pattern 24-2 grid is not adequate to determine the actual boundaries of progressing regions. The limited spatial resolution of the current grid may miss early signs of progression that occur as a deepening of existing scotomas or as an expansion of a scotoma to locations proximal to existing defects.[17,18] If this area were better quantified, progression might be observed earlier. The results and techniques of this study will be used to guide the development of a new thresholding algorithm, SCotoma Oriented PErimetry (SCOPE) that condenses testing locations in visual field areas that are of interest or are at risk, to provide better tracking of progression in a given individual (Paetzold J, et al. *IOVS* 2005;46:ARVO E-Abstract 636).

In conclusion, progressing visual field locations are most likely adjacent to and within a nerve fiber bundle area associated with the visual field defects present in initial tests. Quantifying the spatial relationships of these test locations may be useful in enhancing existing progression algorithms, creating new algorithms, and developing more sensitive, spatially relevant functional tests for follow-up.

References

1. Weber J, Ulrich H. A perimetric nerve fiber bundle map. *Int Ophthalmol*. 1991;15:193–200.
2. Garway-Heath DF, Poinoosawmy D, Fitzke FW, Hitchings RA. Mapping the visual field to the optic disc in normal tension glaucoma eyes. *Ophthalmology*. 2000;107:1809–1815.
3. Anderson DR, Patella VM. *Automated Static Perimetry.* 2nd ed. St. Louis: Mosby, Inc.; 1999.
4. Heijl A, Lindgren A, Lindgren G. Test-retest variability in glaucomatous visual fields. *Am J Ophthalmol*. 1989;108:130–135.
5. Leske MC, Heijl A, Hyman L, Bengtsson B. Early Manifest Glaucoma Trial: design and baseline data. *Ophthalmology*. 1999;106:2144–2153.
6. Fitzke FW, Hitchings RA, Poinoosawmy D, McNaught AI, Crabb DP. Analysis of visual field progression in glaucoma. *Br J Ophthalmol*. 1996;80:40–48.
7. Musch DC, Lichter PR, Guire KE, Standardi CL. The Collaborative Initial Glaucoma Treatment Study: study design, methods, and baseline characteristics of enrolled patients. *Ophthalmology*. 1999;106:653–662.
8. AGIS A. Advanced Glaucoma Intervention Study. 2. Visual field test scoring and reliability. *Ophthalmology.* 1994;101:1445–1455.
9. Spry PG, Johnson CA. Identification of progressive glaucomatous visual field loss. *Surv Ophthalmol*. 2002;47:158–173.
10. Mills RP, Budenz DL, Lee PP, et al. Categorizing the stage of glaucoma from pre-diagnosis to end-stage disease. *Am J Ophthalmol*. 2006;141:24–30.
11. Blumenthal EZ, Sapir-Pichhadze R. Misleading statistical calculations in far-advanced glaucomatous visual field loss. *Ophthalmology*. 2003;110:196–200.
12. Heijl A, Lindgren G, Olsson J, Asman P. Visual field interpretation with empiric probability maps. *Arch Ophthalmol*. 1989;107:204–208.
13. Mooney CZ. *Monte Carlo Simulation.* Thousand Oaks, CA: SAGE Publications, Inc.; 1997:103.
14. Weber J, Dannheim F, Dannheim D. The topographical relationship between optic disc and visual field in glaucoma. *Acta Ophthalmol* (*Copenh*). 1990;68:568–574.
15. Gardiner SK, Crabb DP, Fitzke FW, Hitchings RA. Reducing noise in suspected glaucomatous visual fields by using a new spatial filter. *Vision Res*. 2004;44:839–848.
16. Sample PA, Boden C, Zhang Z, et al. Unsupervised machine learning with independent component analysis to identify areas of progression in glaucomatous visual fields. *Invest Ophthalmol Vis Sci*. 2005;46:3684–3692.
17. Mikelberg FS, Drance SM. The mode of progression of visual field defects in glaucoma. *Am J Ophthalmol*. 1984;98:443–445.
18. Boden C, Blumenthal EZ, Pascual J, et al. Patterns of glaucomatous visual field progression identified by three progression criteria. *Am J Ophthalmol*. 2004;138:1029–1036.